

Effect of strain on electrochemical performance of Janus MoSSe monolayer anode material for Li-ion batteries: First-principles study

Guoqing Wang(王国庆), Wenjing Qin(秦文静), and Jing Shi(石晶)
Citation: Chin. Phys. B, 2021, 30 (**4**): 046301. DOI: 10.1088/1674-1056/abca24
Journal homepage: http://cpb.iphy.ac.cn; http://iopscience.iop.org/cpb

What follows is a list of articles you may be interested in

Two-dimensional MnN utilized as high-capacity anode for Li-ion batteries

Junping Hu(胡军平), Zhangyin Wang(王章寅), Genrui Zhang(张根瑞), Yu Liu(刘宇), Ning Liu(刘宁), Wei Li(李未), Jianwen Li(李健文), Chuying Ouyang(欧阳楚英), and Shengyuan A. Yang(杨声远)
Chin. Phys. B, 2021, 30 (**4**): 046302. DOI: 10.1088/1674-1056/abdda8

First-principles study of the co-effect of carbon doping and oxygen vacancies in ZnO photocatalyst

Jia Shi(史佳), Lei Wang(王蕾), and Qiang Gu(顾强)
Chin. Phys. B, 2021, 30 (**2**): 026301. DOI: 10.1088/1674-1056/abc0db

Electronic structure and optical properties of Ge-and F-doped α -Ga_2O_3: First-principles investigations

Ti-Kang Shu(束体康), Rui-Xia Miao(苗瑞霞), San-Dong Guo(郭三栋), Shao-Qing Wang(王少青), Chen-He Zhao(赵晨鹤), and Xue-Lan Zhang(张雪兰)
Chin. Phys. B, 2020, 29 (**12**): 126301. DOI: 10.1088/1674-1056/abbbff

Surface-regulated triangular borophene as Dirac-like materials from density functional calculation investigation

Wenyu Fang(方文玉), Wenbin Kang(康文斌), Jun Zhao(赵军), Pengcheng Zhang(张鹏程)
Chin. Phys. B, 2020, 29 (**9**): 096301. DOI: 10.1088/1674-1056/ab9bff

First-principles study of structural, mechanical, and electronic properties of W alloying with Zr

Ning-Ning Zhang(张宁宁), Yu-Juan Zhang(张玉娟), Yu Yang(杨宇), Ping Zhang(张平), Chang-Chun Ge(葛昌纯)
Chin. Phys. B, 2019, 28 (**4**): 046301. DOI: 10.1088/1674-1056/28/4/046301

Effect of strain on electrochemical performance of Janus MoSSe monolayer anode material for Li-ion batteries: First-principles study*

Guoqing Wang(王国庆)[1,2], Wenjing Qin(秦文静)[1], and Jing Shi(石晶)[1,†]

[1] Department of Physics, Jiangxi Normal University, Nanchang 330022, China
[2] Institute of Fundamental and Frontier Sciences, University of Electronic Science and Technology of China, Chengdu 610054, China

(Received 29 July 2020; revised manuscript received 16 October 2020; accepted manuscript online 13 November 2020)

First-principles calculations are performed to investigate the effect of strain on the electrochemical performance of Janus MoSSe monolayer. The calculation focuses on the specific capacity, intercalation potential, electronic structure, and migration behavior of Li-ion under various strains by using the climbing-image nudged elastic band method. The result shows that the specific capacity is nearly unchanged under strain. But interestingly, the tensile strain can cause the intercalation potential and Li-ion migration energy barrier increase in MoSSe monolayer, whereas the compressive strain can lead to the intercalation potential and energy barrier decreasing. Thus, the rate performance of the MoSSe anode is improved. By analyzing the potential energy surface of MoSSe surface and equilibrium adsorption distance of Li-ion, we explain the physical origin of the change in the intercalation potential and migration energy barrier. The increase of MoSSe potential energy surface and the decrease of adsorption distance caused by tensile strain are the main reason that hinders Li-ion migration.

Keywords: Janus MoSSe monolayer, strain effect, specific capacity, migration behavior

PACS: 63.20.dk, 62.25.–g, 73.22.–f **DOI:** 10.1088/1674-1056/abca24

1. Introduction

Two-dimensional (2D) materials represented by graphene have received tremendous research enthusiasm.[1–9] Among many 2D materials, transition metal dichalcogenides (TMDs), MX_2 (M = Mo and W; X = S, Se, and Te),[5,10–14] have emerged in recent years due to their moderate direct band gap, good electronic transport properties, and the coupled spin-valley property.[5,11] Recently, researchers have successfully synthesized new MoS_2-like TMDs by chemical vapor deposition, 2D Janus MoSSe. Due to the broken in-plane mirror symmetry, Janus MoSSe possesses the out-of-plane dipole absent in conventional monolayer TMDs.[15,16] Thereupon, a variety of properties of Janus MoSSe monolayer[17] or multilayer MoSSe[18,19] have been widely studied, including electronic structures,[20–22] magnetism,[23,24] phonon transports,[25] photocatalysts,[26–28] and so forth. Unique properties of MoSSe engender a versatility that has a potential application and enabled its use in a wide range of scientific fields, such as thermoelectrics,[29] optoelectronics.[30]

In addition, Janus MoSSe monolayer is a potential anode material and has appeared in the field of ion battery in recent years.[31–33] Shang *et al.*[31] calculated the energy barriers of Li-ion on MoSSe surface and suggested that the rate performance of the Janus MoSSe monolayer is comparable to that of graphene and silicene. Zhou *et al.*[32] reported that heterostructures composed of Janus MoSSe monolayer and graphene as promising anode materials for LIBs. The maximum lithium storage capacity of the heterostructure can be enhanced to 390 mAh/g. And then, He *et al.*[33] experimentally verified that MoSSe with anion vacancies introduced in situ had been achieved for the first time. The anion vacancies in MoSSe could enhance the electronic conductivity, induce more active sites, and obtain better ion storage performance. Verified through the above works, MoSSe has a bright future to serve as anode material.

However, previous studies focused on the lithiation reaction in Janus MoSSe anode under zero strain condition. It is well known that the external strain can be easily implemented by introducing a specific substrate in the fabrication of Janus MoSSe monolayer.[34,35] Furthermore, deformation and stress induced by insertion/extraction of Li in electrode materials during the charging/discharging cycle process,[36] which lead the 2D Janus MoSSe monolayer to form buckling or puckered structures, and will affect the electrochemical performance of the electrode. Recent theoretical works explored the effect of strain on the electrochemical performance of 2D electrode materials. For example, Ge *et al.*[37] systematically studied the effects of strain on the electron-phonon coupling and phonon finite mobility of SnO by using first-principles calculations. Their results show that the compressive strain in the SnO monolayer results in a conduction band minimum (CBM) consisting of two valleys at the Γ point and along the M–Γ line. Hao *et al.*[38] investigated Li-ion diffusion on strained graphene by using first-principles calculations; the re-

*Project supported by the Education Department of Jiangxi Province, China (Grant No. GJJ160337).
†Corresponding author. E-mail: shijing_scu@163.com
© 2021 Chinese Physical Society and IOP Publishing Ltd

sults show that the diffusion coefficient of Li-ion on the plane of stretched graphene is gently reduced compared to without strain, and the effect strongly depends on the magnitude of the strain. Wang *et al.*[39] studied the adsorption property of Li atoms on C_3N under various strains by first-principles method. Hao *et al.*[40] applied the density functional theory calculations to study the strain effect on the Li-ion diffusion and electronic structure of MoS_2; the result shows that the strain can improve electric conductivity that may benefit charge carrier transport. However, to the best of our knowledge, theoretical studies of the effect of different external biaxial strains on the properties of the Janus MoSSe as an anode material for LIBs are scarce. Thus, it is meaningful to study the influence of the electrochemical performance of Janus MoSSe monolayer under strain.

In this work, we explore the specific capacity, intercalation potential, electronic structures, and electrochemical kinetics of Janus MoSSe monolayer under external strain by using first-principles calculation method. We find that the change of strain has little effect on the maximum storage of Li-ion and the interaction potential. But interestingly, the electrochemical kinetics of Janus MoSSe monolayer will change greatly under different strains. Our results will reveal the Li-ion migration mechanism under strain on the surface of MoSSe and evaluate the strain effect on the charge/discharge process Janus MoSSe monolayer as the anode of LIBs. Our results can help to study MoSSe as an anode for LIBs.

2. Methodology

In this paper, all the calculations are performed by using the Vienna *ab initio* simulation package (VASP) based on density functional theory (DFT).[41] The projector augmented wave (PAW) method is used, and the exchange-correlation effect among electrons is described with generalized gradient approximation (GGA), specifically the functional proposed by Perdew–Burke–Ernzerhof (PBE).[42,43] The Li $1s^1 2s^1 2p^1$, Mo $4p^6 5s^1 4d^5$, S $3s^2 3p^4$, and Se $4s^2 4p^4$ electrons are considered as valence electrons. For the plane-wave basis expansion, a cutoff energy of 500 eV is applied to the wave function. In order to describe the interactions between the adsorbed host 2D materials and Li-ions, a damped van der Waals (vdW) correction (DFT-D2) has been added to the DFT exchange-correlation functional to incorporate the effect of nonbonding forces.[44,45] The lattice parameters and the ionic positions are fully relaxed until the net force on each atom is less than 0.02 eV/Å. The convergence criterion of the total energy is 10^{-5} eV per atom. The Janus MoSSe monolayer is separated with a 20 Å vacuum layer in the z-axis direction to avoid the interaction between the periodically repeated structures. We utilize the Monkhorst–Pack k-points mesh of $11 \times 11 \times 1$ for primitive cell and $5 \times 5 \times 1$ for 3×3 supercell in the structural optimization and other calculations. To study the Li-ion lateral migration on the MoSSe monolayer surface, the climbing-image nudged elastic band (CI-NEB) method[46] is employed to determine the Li-ion migration path and evaluate the energy barrier. The spring constant is set to -5. Five images are interpolated between the initial and the final states along each pathway in our calculation. The phonon frequencies are calculated by using PHONOPY code,[47] which can directly use the force constant (Hessian matrix) calculated by DFPT,[48] as also implemented in VASP.

Generally, the adsorption energy E_{ad} is essential for understanding the Li-ion adsorption strength on the 2-D host material. Thus, the amount of Li-storage on the MoSSe monolayer can be evaluated by the sequential adsorption energy, which is defined as

$$E_{\mathrm{ad}} = E_{\mathrm{host}+(n+1)\mathrm{Li}} - E_{\mathrm{host}+n\mathrm{Li}} - E_{\mathrm{Li}}, \tag{1}$$

where $E_{\mathrm{host}+(n+1)\mathrm{Li}}$ and $E_{\mathrm{host}+n\mathrm{Li}}$ are the optimized total ground state energies of the 2-D host with $(n+1)$ and n Li-ions adsorbed, respectively. E_{Li} is the total energy of an isolated Li atom. According to the definition of Eq. (1), negative adsorption energy indicates that Li-ions are bound to the 2-D host.

The intercalation potential is positive when the adsorption energy is lower than the cohesive energy of the body-centered cubic (BCC) phase Li-metal. Otherwise, from the thermodynamical point of view, the formation of a Li dendrite is favorable when the intercalation potential becomes negative. Therefore, the theoretical capacity of the 2-D MoSSe monolayer can be evaluated by sequential adsorption energy. The maximum theoretical capacity (C_{M}) can be estimated by the equation

$$C_{\mathrm{M}} = \frac{xF}{M_{\mathrm{MoSSe}}}, \tag{2}$$

where x, F, and M_{MoSSe} are the maximum value of electrons during the electrochemical process, the Faraday constant, and the mass of M_{MoSSe}, respectively.

To further understand the sequential adsorption energy, the intercalation potential V has been evaluated as follows:

$$V = -\frac{E_{\mathrm{Li}_{x_2}\mathrm{host}} - E_{\mathrm{Li}_{x_1}\mathrm{host}} - (x_2 - x_1)E_{\mathrm{Li}}}{(x_2 - x_1)e}, \tag{3}$$

where $E_{\mathrm{Li}_{x_2}\mathrm{host}}$, $E_{\mathrm{Li}_{x_1}\mathrm{host}}$, and E_{Li} are the total energies of the Li_{x_2} host, Li_{x_1} host, and BCC phase Li metal, respectively. According to this formula, a positive potential indicates energetically favorable intercalation.

3. Results and discussion

3.1. The strain effect on structures of the monolayer Janus MoSSe

The primitive unit cell of MoSSe monolayer is a flat hexagonal lattice with a space group of $P6_3/mmc$ (No. 194).

The S and Se atoms take the 4f Wyckoff position, while the Mo atoms take the 2c Wyckoff position, as shown in Fig. 1(a). The corresponding equilibrium lattice constant is 3.260 Å, and the optimized Mo–S and Mo–Se bond lengths are 2.423 Å and 2.539 Å, respectively. The thickness of the Janus MoSSe monolayer triple layers is 3.231 Å, which is in good agreement with other results.[18,21] The supercell lattice constants of MoSSe, $Li_{1/9}$MoSSe, $Li_{2/9}$MoSSe, Li_1MoSSe, and Li_2MoSSe are 9.780 Å, 9.868 Å, 9.897 Å, 9.918 Å, and 10.025 Å, respectively. Then we apply a compressive or tensile biaxial strain in Janus MoSSe monolayer, varying from −6% to 6% with an interval of 2%, which is readily achievable strain range in real experiments.[49,50] Here, the strain (ε) is defined as the ratio between the change of lattice constant ($a - a_0$) and the equilibrium lattice constant (a)

$$\varepsilon = (a - a_0)/a. \tag{4}$$

A positive value means a tensile strain, while a negative one means a compressive strain. To verify the stability of MoSSe under different strains, we calculated the phonon spectra of MoSSe. The phonon band structure of MoSSe is extracted from a $3 \times 3 \times 1$ supercell. Figure 1(b) shows the calculated phonon dispersions relation under −6%, 0%, and 6% strain. We also tested other strain values; please refer to ESI†, Fig. S1. As shown in Fig. 1(b), the phonon spectra of the structure under −6% and 6% strain show no imaginary frequency in the Brillouin zone of MoSSe monolayer, confirming the stability and thus the possibility of experimental realization.

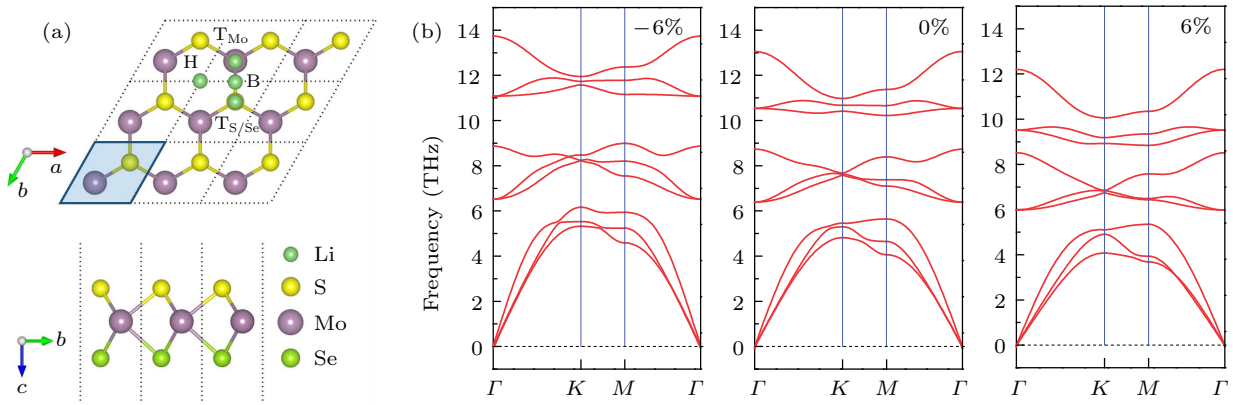


Fig. 1. (a) Top and side views of MoSSe monolayer with $3 \times 3 \times 1$ supercell, and Li-ion adsorption sites on the MoSSe surface. The unit cell is indicated by the parallelogram. Green, yellow, purple, and emerald balls represent Li, S, Mo, and Se atoms, respectively. (b) Phonon dispersions of the MoSSe monolayer under −6%, 0%, and 6% strain, respectively.

3.2. The effect of strain on the lithium storage performance

3.2.1. The effect of strain on the specific capacity

To explore the effect of the strain on the specific capacity of Li-ion, we investigated the adsorption behavior of Li-ion on the Janus monolayer MoSSe under different strains.

First, we evaluate the adsorption sites and the maximum adsorption capacity of Li-ion on the Janus MoSSe monolayer supercell without strain. For the upper and lower surfaces of the monolayer MoSSe supercell cell, six adsorption sites are available. They are top site of Mo atom (denoted as T_{Mo}), top site of S/Se atom (denoted as $T_{S/Se}$), and hollow site (denoted as H) on the side of the S layer or Se layer, as shown in Fig. 1(a). For one Li-ion adsorption, there are six adsorption configurations. After full geometry relaxation, depending on the definition of the adsorption energy in Eq. (1), we calculated the adsorption energy of these six adsorption configurations and listed in Table 1. Results show that the adsorption energy at the T_{Mo} site on both the side of the S and Se layer is larger than those at the $T_{S/Se}$ and hollow site, especially the T_{Mo} site on the side of the S layer (−2.442 eV). It indicated that Li-ion prefers staying at the T_{Mo} site on the S layer.

Table 1. Adsorption energies (eV) for all Li-adsorption sites of the monolayer MoSSe.

	Top site on Mo (T_{Mo})	Top site on S/Se ($T_{S/Se}$)	Hollow site (H)
S side	−2.442	−1.522	−2.288
Se side	−1.774	−0.978	−1.621

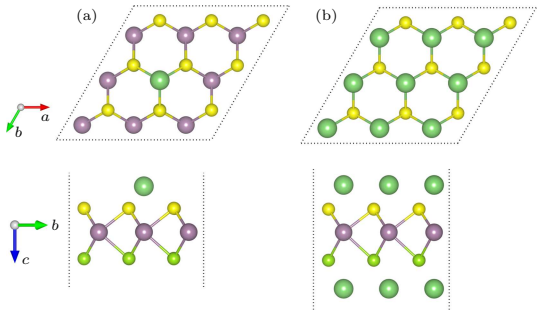


Fig. 2. Top view and side view of the atomic structures of (a) $Li_{1/9}$MoSSe and (b) Li_2MoSSe.

In order to calculate the maxNum adsorption capacity of a $3 \times 3 \times 1$ supercell of monolayer MoSSe for Li-ion, according to Eq. (1), we calculated the sequential adsorption energies of adsorption configurations (Li_xMoSSe) by gradually increasing the amount of Li-ion adsorbed. Our results indicate that the T_{Mo} site on the side of the S layer is the first choice for Li-ion

adsorption. So, when more Li-ions are introduced, they prefer to stay on the S layer, until all sites are fully occupied, corresponding to $Li_{1/9}MoSSe$ (see Fig. 2(a)). And then, Li ions start to occupy the T_{Mo} site on the side of the Se layer, until all the T_{Mo} of the S and Se layer are fully occupied by Li-ions, corresponding to Li_2MoSSe (see Fig. 2(b)). In this adsorption configuration with the adsorption energies close to the cohesive energy of the BCC phase Li-metal (−1.999 eV/atom calculated with the GGA-PBE potential in this study). Generally, if the adsorption energy is lower than −1.999 eV/atom, Li-ion adsorption on the host is favored, corresponding to a positive discharge potential. Otherwise, Li-metal formation is favored, and discharge potential is negative. Thus, a $3 \times 3 \times 1$ supercell of monolayer MoSSe can store as many as 18 Li-ions, corresponding to Li_2MoSSe, as shown in Fig. 2(b). The corresponding theoretical capacity is 258.8 mAh/g by Eq. (2).

Second, we investigated the adsorption behavior of Li atom on the Janus monolayer MoSSe under strain. Similar to section 1, we first examined the adsorption sites of Li atom under strain. The result shows that the Li-ion still prefers staying at the T_{Mo} site on the S layer. Whereafter, we calculated the sequential adsorption energies of Li_xMoSSe under the strains ranging from −6% to 6%. In order to facilitate comparison, the adsorption energy of Li_xMoSSe against strain and Li-ion concentration is shown in Fig. 3. The black triangle, red circle, and blue square in Fig. 3 represent the adsorption energy of Li_xMoSSe under −6%, 0%, and 6% strain, respectively. As can be seen from Fig. 3, the adsorption energies decrease with the Li-ion concentration. This is because the attractive interaction between Li-ions and the host (MoSSe) decreases and the repulsive interactions between the adsorbed Li-ions increase. Interestingly, we can see that the effect of strain on adsorption energy is very small, especially $Li_{1/9}MoSSe$ and Li_2MoSSe, there is almost no effect.

In addition, we calculated the intercalation potential V by Eq. (3). The intercalation potentials are presented in Table 2. As shown in Table 2, when the Li content x is less than 2, the intercalation potential V ranges from 0.123 to 1.205 V under −6% compressive strain, 0.034 to 0.442 V without strain, and 0.057 to 0.410 V under 6% tensile strain. The intercalation potential V under other strains is also calculated; please refer to ESI†, Table S1. But when x is greater than 2, the intercalation potential V becomes negative. So, at the maximum unit Li adsorption capacity, the insertion phase is still Li_2MoSSe with strain. The corresponding theoretical specific capacity of the Janus monolayer MoSSe still is 258.8 mAh/g. In sum, both compressive and tensile stresses have no effect on the theoretical specific capacity of the Janus monolayer MoSSe. Comparing with 1.0 V for carbon (Li_xC_6) and 1.12 V for graphite,[51] MoSSe is suitable for anode electrode with such a small intercalation potential (0.442–0.034 V).

Table 2. Intercalation potentials V on MoSSe as functions of the Li content in Li_xMoSSe under strain (unit: V).

Strain	x				
	1/9	2/9	1	2	19/9
−6%	1.205	0.396	0.204	0.123	−0.294
0%	0.442	0.172	0.133	0.034	−0.218
6%	0.410	0.616	0.214	0.057	−0.550

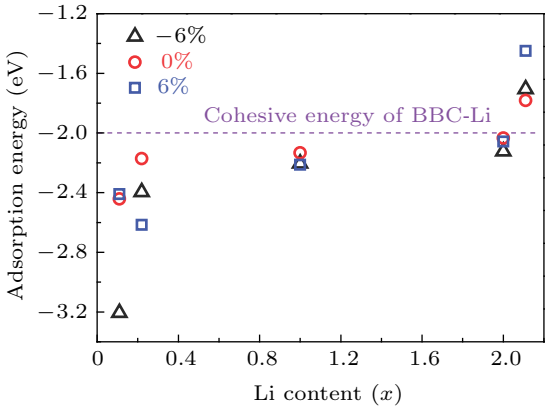


Fig. 3. The sequential adsorption energies as the function of Li content in the Li_xMoSSe under strain. Black triangles, red circles, and blue squares represent the adsorption energy of Li_xMoSSe under −6%, 0%, and 6% strain, respectively.

To study the strain effects on the interaction between Li-ion and the host (MoSSe) and understand the physical origin of the no change in adsorption energy, we calculated the equilibrium adsorption distance of Li-ion adsorption on MoSSe. Taking $Li_{1/9}MoSSe$ and Li_2MoSSe as examples, the adsorption distance against various strains are presented in Figs. 4(a) and 4(b). We can see that the adsorption distance of Li on Se surface of MoSSe is less than that on S surface, and the adsorption distance of Li increases under compressive strain and decreases under tensile strain, for the side of the S and Se layer in $Li_{1/9}MoSSe$ and Li_2MoSSe. This is not consistent with the change of adsorption energy.

Whereafter, we calculated the charge transfer of Li-ion adsorption on MoSSe under strain by the Bader charge analysis method.[52] The analysis results are presented in Figs. 4(c) and 4(d). The Bader charge of pure MoSSe monolayer under different strains; please refer to ESI†, Fig. S2. A negative value indicates charge depletion, while a positive value represents charge accumulation. As seen from Figs. 4(c) and 4(d), the electron gaining ability of S atom is greater than that of Se, corresponding to that the adsorption distance of the side of S layer is smaller than that of the side of Se layer for the Li-ion. It was found that the charge transfer of Li atom hardly changes with strain. The charge depletion of Li atom is −0.888 *e*/per atom for $Li_{1/9}MoSSe$, and with −0.770 *e*/per atom for Li_2MoSSe. Therefore, the strain induced charge transfer is mainly between the elements of the adsorbent, i.e.,

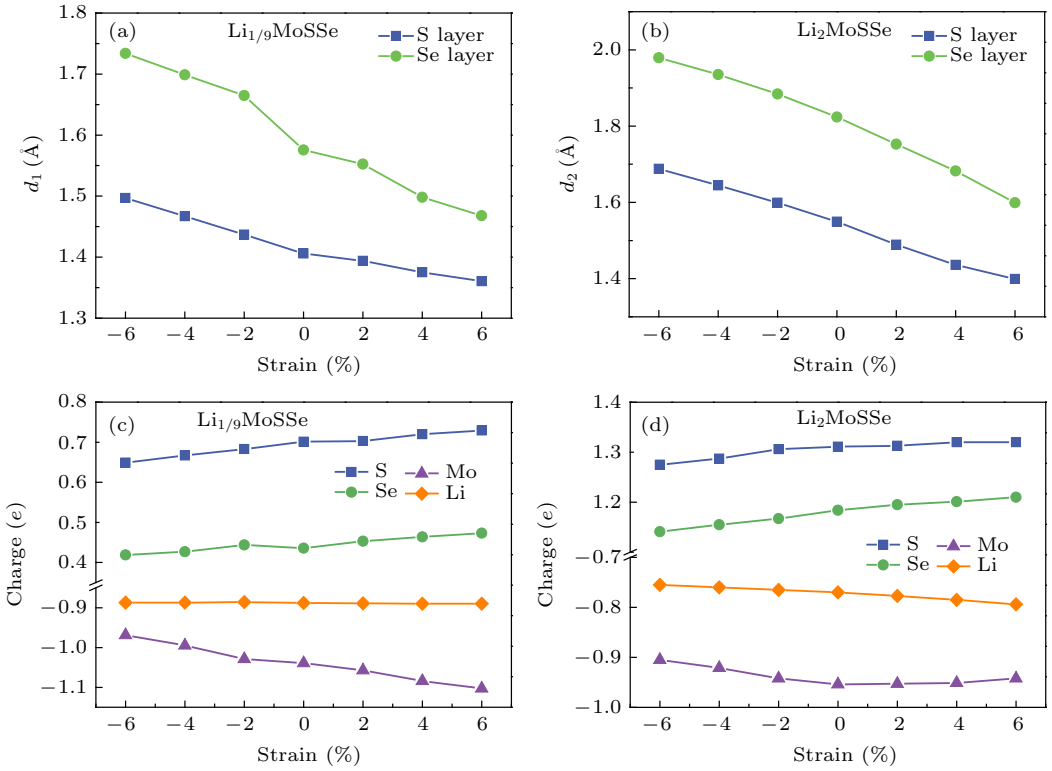


Fig. 4. The equilibrium adsorption distance of Li-ion on (a) $Li_{1/9}MoSSe$ and (b) Li_2MoSSe under different strains. The gain or loss of Li, Mo, S, and Se atoms in (c) $Li_{1/9}MoSSe$ and (d) Li_2MoSSe with compressive, without, and with tensile strains (unit: *e*/per atom).

Mo, S, and Se. The nature of adsorption is the electrostatic attraction between Li and MoSSe. The attraction of S and Se to Li is the main reason for the increase of the adsorption energy, while the repulsion of Mo is the main reason for the decrease of the adsorption energy. When the strain is applied, although the number of electron gain of S and Se atom increases with the strain, the electron loss of Mo atom also increases with the strain, causing both attraction and repulsion to increase. Accordingly, the adsorption energy barely relies on the strain.

3.2.2. The effect of strain on electronic structures of lithiated monolayer MoSSe

To study the strain effects on the electronic properties, we calculated the total density of states (TDOS) of the adsorption phases Li_xMoSSe, from which we can learn more about the physical origin of the strain effect. Figure 5 shows the TDOS of MoSSe, $Li_{1/9}MoSSe$, and Li_2MoSSe under various strains. As shown in the dark gray area in Fig. 5, we have found that MoSSe is a semiconductor with a band gap of 1.018 eV. When a −6% strain is applied, TDOS of MoSSe shows that the energy gap is slightly reduced to 0.768 eV, whereas a 6% tensile strain is applied, TDOS of MoSSe shows the band gap disappears and reaches a metallic state, which may be a great benefit to charge carrier transport for potential applications in ion batteries and other electronic devices. When Li atoms are adsorbed, the density of states at the Fermi level increases with the Li contents, leading to increasingly metallic properties of Li_xMoSSe, as shown in Fig. 5. This indicates that Li atom provides more active electrons. It is noteworthy that both compressive and tensile stresses have little effect on the density of states of Li_xMoSSe at the Fermi level. The DOS of $Li_{1/9}MoSSe$ and Li_2MoSSe under other strains are tested; please refer to ESI†, Fig. S3.

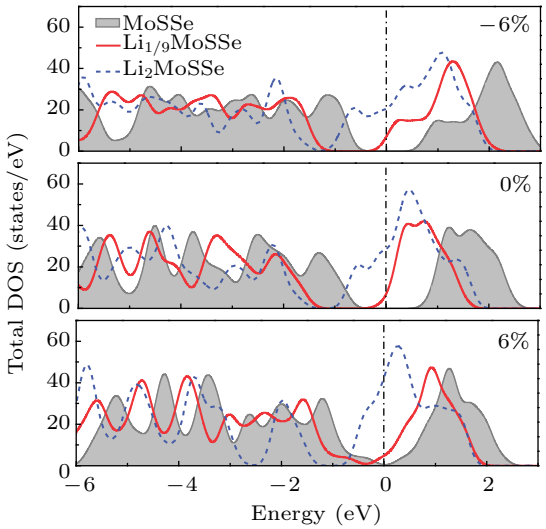


Fig. 5. TDOS of Janus MoSSe monolayer, $Li_{1/9}MoSSe$ and Li_2MoSSe.

3.2.3. The effect of strain on Li-ion diffusion on monolayer MoSSe

Diffusion of Li-ion on MoSSe surface plays a key role in circuit rate performance of batteries. To investigate the strain effects on the Li-ion diffusion on MoSSe surface, we calculated the Li-ion migration on MoSSe without strain and

with −6%, 6% of strain by CI-NEB method. As we know, the diffusion coefficient and migration energy barrier of Li-ion are dependent on Li concentrations. For simplicity, here we study two extreme cases: Li-ion and Li-vacancy migration, corresponding to the Li diffusion behavior in Li-poor state ($Li_{1/9}$MoSSe) and Li-rich phase ($Li_{17/9}$MoSSe), respectively. Figures 6 and 7 show the migration paths and energy barriers of one Li-ion and Li-vacancy migration on the MoSSe with −6%, 0%, and 6% strain. For other strain's values, please refer toESI†, Figs. S4 and S5.

For the case of Li-ion migration, without strain, we can see that Li-ion migrates from the most stable T_{Mo} site to the nearest neighbor T_{Mo} site through a metal-stable site (H) on both the side of the S layer and Se layer of MoSSe. During this migration process, Li has to overcome an energy barrier of 0.316 and 0.239 eV on the side of the S layer and Se layer of MoSSe (see Fig. 6(c)), respectively. With a −6% compressive strain, Li follows the same migration path, but the energy barriers decrease to 0.267 and 0.216 eV (see Fig. 6(b)). In comparison, the energy barriers of Li ions increase to 0.328 and 0.356 eV with a 6% tensile strain (see Fig. 6(d)).

For the case of Li-vacancy migration, we can see that Li vacancy follows the same migration path on $Li_{17/9}$MoSSe, but the energy barriers have increased. Without strain, as shown in Fig. 7(c), the migration energy of Li vacancy on the S layer and Se layer are 0.581 and 0.364 eV, respectively. There is the same effect of strain on energy barriers of Li vacancy migration, as shown in Figs. 7(b) and 7(d). With −6% of compressive strain, the energy barriers of Li-vacancy on the side of the S layer and Se layer of MoSSe are reduced to 0.403 and 0.297 eV, respectively. The opposite aspect is that the migration energy barriers of Li-vacancy increase to 0.584 and 0.588 eV with 6% of tensile strain.

Figure 8 present the migration energy barriers of Li-ions and Li-vacancy against strain. We can see that the migration barrier on Se surface of MoSSe is lower than that on S surface. This is mainly because the adsorption distance of Li on Se surface of MoSSe is greater than that on S surface, as shown in Figs. 4(a) and 4(b). In the process of Li-ion migration, the electrostatic interaction to be overcome is small. Note that the compressive strain tends to affect the fast diffusion of Li on MoSSe, and the effect of strain on Se surface is greater than that on S surface. For example, the migration energy barriers of Li-ion on the side of S layer decrease from 0.32 eV without strain to 0.26 eV with −6% compressive strain. However, tensile strain turns to increase the migration barrier, especially the migration of Li-vacancy in lithium-rich phase, such as the migration energy barriers of Li-vacancy on the side of Se layer increase from 0.35 eV without strain to 0.56 eV with 6% tensile strain. This can also be explained by the variation of adsorption distances with strains. The adsorption distance increases under compressive strains and decreases under tensile strains. This is not consistent with the effect law of strain on MoS_2. A 6% strain increases the migration barrier of Li-ion on MoS_2 by only 0.01 eV, indicating little influence on Li diffusion.

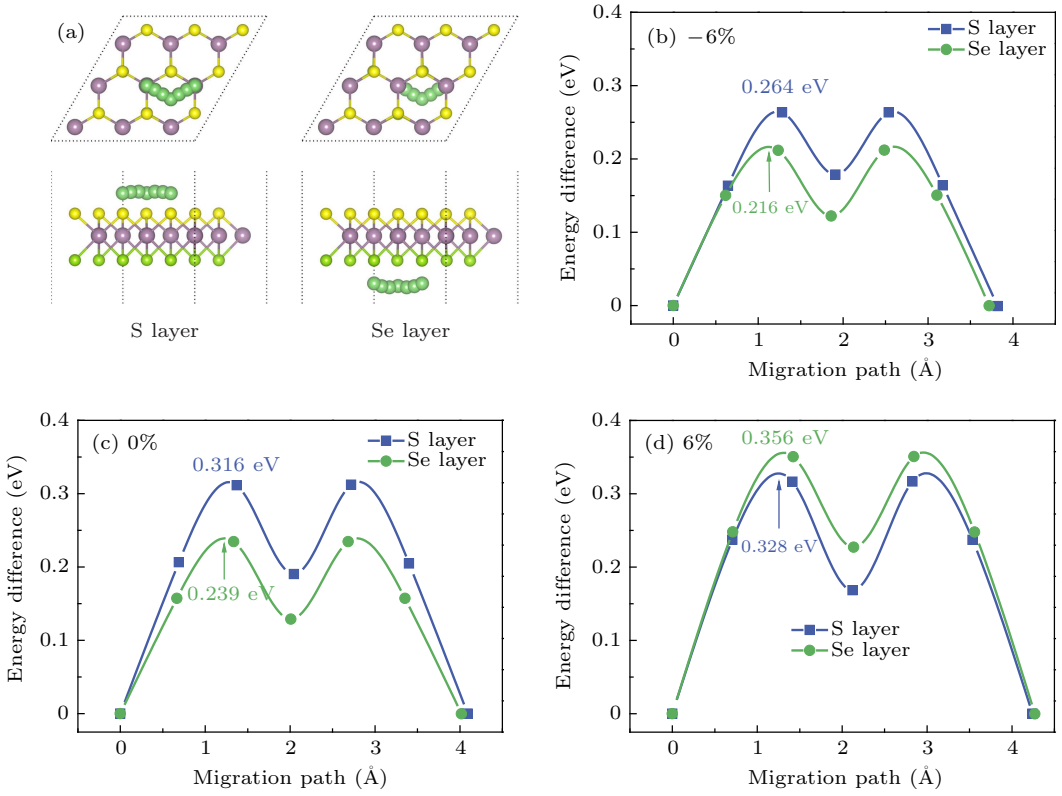


Fig. 6. Migration path and energy barriers: (a) for one Li-ion migration on the MoSSe monolayer, (b)–(c) for energy profile of Li-ion diffusion with −6%, 0%, and 6% strain, respectively.

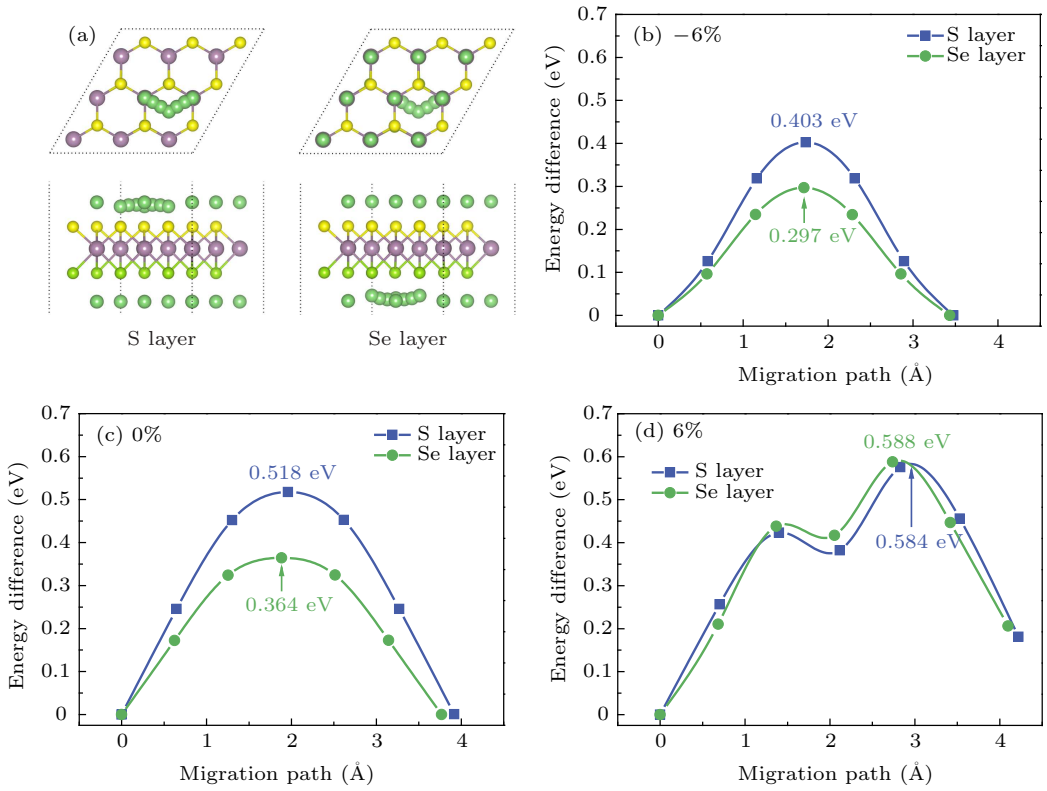


Fig. 7. Migration path and energy barriers: (a) for one Li-vacancy migration on 17 Li adsorbed on the MoSSe monolayer, (b)–(c) for energy profile of Li-vacancy diffusion with −6%, 0%, and 6% strain, respectively.

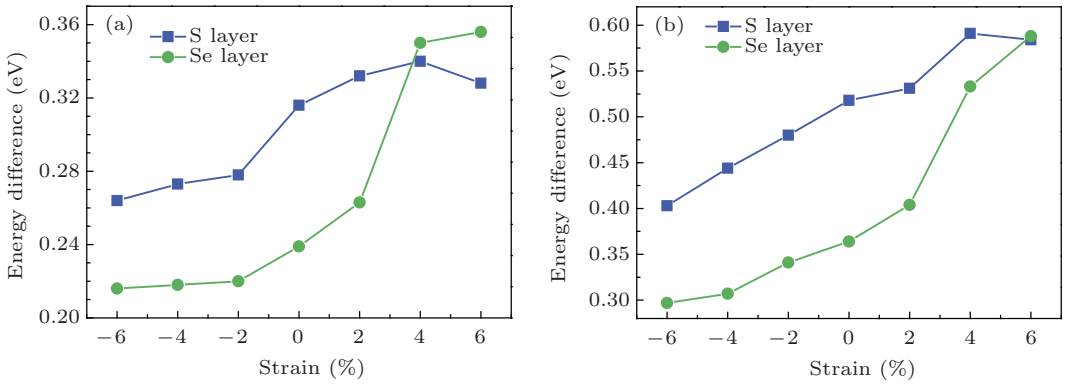


Fig. 8. The variation of (a) one Li-ion and (b) one Li-vacancy migration energy barriers as a function of the applied external strain.

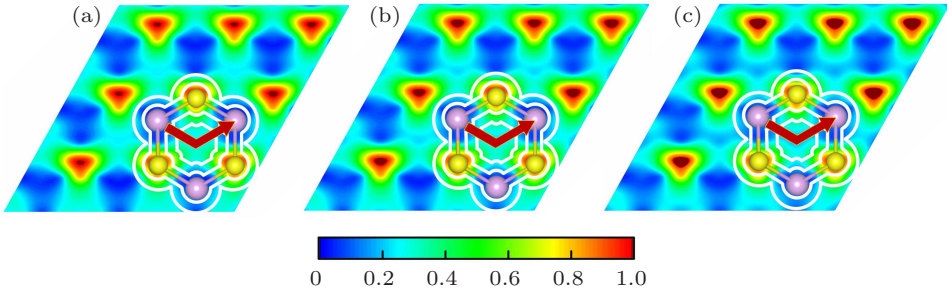


Fig. 9. PES of Li diffusion on Janus MoSSe monolayer with (a) −6%, (b) 0%, and (c) 6% of strain. The red arrow is the minimum energy path of Li migration.

In order to further explain the effect law of strain on the Li migration, we calculated the potential energy surface (PES) of Li diffusion on MoSSe with −6% of strains, without strain, and with 6% of strain. Here, PES is calculated by fixing the adsorbed ions laterally at different positions and allowing all other atoms and the ion height to relax. In our study, we constructed 20 structures along zigzag and armchair directions of MoSSe and optimized a total of 400 structures to obtain the

relative energy with reference to the lowest energy at the most stable adsorption site. Figures 9(a), 9(b) and 9(c) show the PES and Li diffusion path of Li migration on MoSSe under −6%, 0%, and 6% strain, respectively. As shown in Fig. 9, with the increase of tensile strain, a darker color of S site shows a higher PES of S atom. At this time, the color of the blue central region of the six-membered ring composed of Mo and S atoms is gradually deepening from compressive strain to tensile strain, and the part is the minimum energy path of Li-ion. This shows that the PES of the migration path increases with the stress, which leads to the increase of Li-ion migration barrier (see Fig. 9(c)).

4. Conclusion

In summary, we performed systematic first-principles calculations to explore the strain effects on the specific capacity, intercalation potential, electronic structures, and migration behavior of Li-ion on MoSSe in the context of ion batteries. Our results show that both compressive and tensile stresses have little effect on the theoretical specific capacity of the Janus MoSSe monolayer. We have found that strain has a great effect on the electronic structure of MoSSe. For example, when a 6% tensile strain is applied, TDOS of MoSSe shows the band gap disappears and achieves a metallic state, which may be of great benefit to charge carrier transport for potential applications in ion batteries. Strain also has a certain effect on the adsorbed MoSSe (Li_xMoSSe), but the effect is small. For the Li migration behavior, the compressive strain tends to affect the fast diffusion of Li on MoSSe, and the effect of strain on Se surface is greater than that on S surface. This can be explained by the variation of adsorption distance and potential energy surface with strains. Overall, the above results show the prospect of applying strain to energy-related technology and provide theoretical guidance for exploring the effect of strain on electrode materials.

References

[1] Novoselov K S, Jiang D, Schedin F, Booth T J, Khotkevich V V, Morozov S V and Geim A K 2005 *Proc. Natl. Acad. Sci. USA* **102** 10451
[2] Novoselov K S, Geim A K, Morozov S V, Jiang D, Zhang Y, Dubonos S V, Grigorieva I V and Firsov A A 2004 *Science* **306** 666
[3] Geim A K and Novoselov K S 2007 *Nat. Mater.* **6** 183
[4] Wang P, Orimo S, Matsushima T, Fujii H and Majer G 2002 *Appl. Phys. Lett.* **80** 318
[5] Wang Q H, Kalantar-Zadeh K, Kis A, Coleman J N and Strano M S 2012 *Nat. Nanotechnol.* **7** 699
[6] Matte H S S R, Gomathi A, Manna A K, Late D J, Datta R, Pati S K and Rao C N R 2010 *Angew. Chem. Int. Edit.* **49** 4059
[7] Zhang J L, Zhao S, Han C, Wang Z, Zhong S, Sun S, Guo R, Zhou X, Gu C D, Di Yuan K, Li Z and Chen W 2016 *Nano Lett.* **16** 4903
[8] Peng R, Ma Y, He Z, Huang B, Kou L and Dai Y 2019 *Nano Lett.* **19** 1227
[9] Zhang G and Zhang Y W 2017 *Chin. Phys. B* **26** 034401
[10] Mak K F and Shan J 2016 *Nat. Photon.* **10** 216
[11] Hong H, Cheng Y, Wu C, Huang C, Liu C, Yu W, Zhou X, Ma C, Wang J, Zhang Z, Zhao Y, Xiong J and Liu K 2020 *Chin. Phys. B* **29** 077201
[12] Wang H, Feng H and Li J 2014 *Small* **10** 2165
[13] Zeng F, Zhang W B and Tang B Y 2015 *Chin. Phys. B* **24** 097103
[14] Liu J, Ma Y Q, Dai Y W, Chen Y, Li Y, Tang Y N and Dai X Q 2019 *Chin. Phys. B* **28** 107101
[15] Lu A Y, Zhu H, Xiao J, Chuu C P, Han Y, Chiu M H, Cheng C C, Yang C W, Wei K H, Yang Y, Wang Y, Sokaras D, Nordlund D, Yang P, Muller D A, Chou M Y, Zhang X and Li L J 2017 *Nat. Nanotechnol.* **12** 744
[16] Zhang J, Jia S, Kholmanov I, Dong L, Er D, Chen W, Guo H, Jin Z, Shenoy V B, Shi L and Lou J 2017 *ACS Nano* **11** 8192
[17] Ma X, Wu X, Wang H and Wang Y 2018 *J. Mater. Chem. A* **6** 2295
[18] Wei Y, Xu X, Wang S, Li W and Jiang Y 2019 *Phys. Chem. Chem. Phys.* **21** 21022
[19] Song B, Liu L and Yam C 2019 *J. Phys. Chem. Lett.* **10** 5564
[20] Li F, Wei W, Zhao P, Huang B and Dai Y 2017 *J. Phys. Chem. Lett.* **8** 5959
[21] Long C, Dai Y, Gong Z R and Jin H 2019 *Phys. Rev. B* **99** 115316
[22] Zhang X, Song Y, Zhang F, Fan Q, Jin H, Chen S, Jin Y, Gao S, Xiao Y, Mwankemwa N, Jiang L and Zhang W 2019 *Mater. Res. Express* **6** 105055
[23] Peng R, Ma Y, Zhang S, Huang B and Dai Y 2018 *J. Phys. Chem. Lett.* **9** 3612
[24] Guan S S, Ke S S, Yu F F, Deng H X, Guo Y and Lü H F 2019 *Appl. Surf. Sci.* **496** 143692
[25] Guo S D 2018 *Phys. Chem. Chem. Phys.* **20** 7236
[26] Wei S, Li J, Liao X, Jin H and Wei Y 2019 *J. Phys. Chem. C* **123** 22570
[27] Ma X, Yong X, Jian C C and Zhang J 2019 *J. Phys. Chem. C* **123** 18347
[28] Guan Z, Ni S and Hu S 2018 *J. Phys. Chem. C* **122** 6209
[29] Deng S, Li L, Guy O J and Zhang Y 2019 *Phys. Chem. Chem. Phys.* **21** 18161
[30] Guo R, Bu X, Wang S and Zhao G 2019 *New J. Phys.* **21** 113040
[31] Shang C, Lei X, Hou B, Wu M, Xu B, Liu G and Ouyang C 2018 *J. Phys. Chem. C* **122** 23899
[32] Zhou S H, Zhang J, Ren Z Z, Gu J F, Ren Y R, Huang S, Lin W, Li Y, Zhang Y F and Chen W K 2020 *Chem. Phys.* **529** 110583
[33] He H, Huang D, Gan Q, Hao J, Liu S, Wu Z, Pang W K, Johannessen B, Tang Y, Luo J L, Wang H and Guo Z 2019 *ACS Nano* **13** 11843
[34] Li H, Tsai C, Koh A L, Cai L, Contryman A W, Fragapane A H, Zhao J, Han H S, Manoharan H C, Abild-Pedersen F, Norskov J K and Zheng X 2016 *Nat. Mater.* **15** 48
[35] Zhang C, Li M Y, Tersoff J, Han Y, Su Y, Li L J, Muller D A and Shih C K 2018 *Nat. Nanotechnol.* **13** 152
[36] Zhang W J 2011 *J. Power Sources* **196** 13
[37] Ge Y F and Liu Y 2019 *Chin. Phys. B* **28** 077104
[38] Hao F and Chen X 2015 *Mater. Res. Express* **2** 105016
[39] Wang D D, Bao Y, Wu T S, Gan S Y, Han D X and Niu L 2018 *Carbon* **134** 22
[40] Hao J Y, Zheng J F, Ling F L, Chen Y K, Jing H R, Zhou T W, Fang L and Zhou M 2018 *Sci. Rep.* **8** 2079
[41] Kresse G and Furthmüller J 1996 *Phys. Rev. B* **54** 11169
[42] Blöchl P E 1994 *Phys. Rev. B* **50** 17953
[43] Kresse G and Joubert D 1999 *Phys. Rev. B* **59** 1758
[44] Grimme S 2006 *J. Comput. Chem.* **27** 1787
[45] Grimme S, Antony J, Ehrlich S and Krieg H 2010 *J. Chem. Phys.* **132** 154104
[46] Henkelman G, Uberuaga B P and Jónsson H 2000 *J. Chem. Phys.* **113** 9901
[47] Togo A and Tanaka I 2015 *Scripta Mater.* **108** 1
[48] Baroni S, De Gironcoli S, Dal Corso A and Giannozzi P 2001 *Rev. Mod. Phys.* **73** 515
[49] Bertolazzi S, Brivio J and Kis A 2011 *ACS. Nano* **5** 9703
[50] Castellanos-Gomez A, Poot M, Steele G A, van der Zant H S J, Agrait N and Rubio-Bollinger G 2012 *Adv. Mater.* **24** 772
[51] Goodenough J B and Kim Y 2010 *Chem. Mater.* **22** 587
[52] Henkelman G, Arnaldsson A and Jónsson H 2006 *Comp. Mater. Sci.* **36** 354